

Quantum Entangled States of a Classically Radiating Macroscopic Spin

Ori Somech[✉] and Ephraim Shahmoon^{*}

Department of Chemical & Biological Physics, Weizmann Institute of Science, Rehovot 7610001, Israel



(Received 12 June 2023; accepted 23 February 2024; published 21 March 2024)

Entanglement constitutes a main feature that distinguishes quantum from classical physics. Here, however, we show that entanglement may also serve as the essential ingredient for the emergence of classical behavior in a radiating spin system. We consider the relation between the state of a macroscopic spin, such as an atomic ensemble, and the radiation it emits. We introduce a new class of macroscopic spin states, the coherently radiating spin states (CRSSs), defined as the asymptotic eigenstates of the SU(2) lowering operator. We find that a spin emitter in a CRSS radiates classical coherent light, although the CRSS itself is a quantum entangled state exhibiting spin squeezing. We further show that the CRSS is naturally realized in Dicke superradiance and underlies the dissipative Dicke phase transition, hence predicting the optimal scaling of spin squeezing in superradiance. More generally, the CRSS emerges as the ground state of a collective spin Hamiltonian. The CRSS thus provides a promising concept for studying many-body spin systems in various platforms, with applications ranging from quantum metrology and lasing to phase transitions.

DOI: 10.1103/PRXQuantum.5.010349

I. INTRODUCTION

Various platforms in quantum research, such as those comprising ensembles of atoms or artificial quantum emitters, are characterized by a collective macroscopic spin. A common goal is the study of quantum correlated states within the macroscopic spin itself or in the light it radiates, with applications ranging from quantum metrology [1–4] and ultranarrowband lasers [5–7], to the exploration of superradiance [8–17] and dissipative many-body systems [18–21]. This endeavor raises the question of the relation between quantum correlations in the spin system and those in the radiated light, and, in particular, of the classical limit of a macroscopic-spin emitter.

We address these questions by considering an SU(2) spin- j , such as that describing the collective dipole formed by N two-level, atomlike emitters ($N = 2j \gg 1$). Focusing first on the spin degrees of freedom, classical behavior of this macroscopic spin is typically associated with coherent spin states (CSSs) [22–24]. These are characterized by an average spin of length $j \gg 1$ along a certain direction and a minimal uncertainty circle perpendicular to it [Fig. 1(a)] [25]. Moreover, a CSS contains no

entanglement: it is a product state of the $N = 2j$ constituent atoms. Nevertheless, unlike what one may expect [22], we find below that a macroscopic spin in a CSS does not act as a classical radiating dipole: it emits quantum correlated light rather than coherent-state light, the latter being associated with the classical limit of radiation [10,26,27].

In contrast, here we introduce the *coherently radiating spin state* (CRSS) as the state of a spin system that produces classical-like coherent state radiation [Fig. 1(b)]. We find that such states exist in the macroscopic limit $j \gg 1$ and are given by the approximate eigenstates of the spin lowering operator $\hat{J}_- = \hat{J}_x - i\hat{J}_y$ with continuous complex eigenvalues α restricted to $|\alpha| < j$. We show that the CRSS possesses several interesting features. (1) It is a nonclassical state exhibiting spin squeezing that increases as $|\alpha| \rightarrow j$. For a spin- j describing $N = 2j$ two-level atoms, this means that the constituent atoms are pairwise entangled [23,28,29]. (2) The CRSS generically exhibits a “magnetization” phase transition at $|\alpha| = j$. (3) The CRSS is naturally realized as the steady state of driven-dissipative Dicke superradiance [18,30–35], and is at the origin of the dissipative Dicke phase transition [18,19,21,30,31,36]. This allows us to find new analytical predictions such as the scaling $N^{-1/3}$ of the best achievable spin squeezing in superradiance. (4) The radiated light from a CRSS is a coherent state, whose amplitude is proportional to α . For superradiance, this leads to the prediction that the macroscopic spin dipole, although being a highly nonlinear quantum system, scatters light just like a linear classical system. The CRSS then forms a remarkable

* ephraim.shahmoon@weizmann.ac.il

Published by the American Physical Society under the terms of the [Creative Commons Attribution 4.0 International license](#). Further distribution of this work must maintain attribution to the author(s) and the published article's title, journal citation, and DOI.

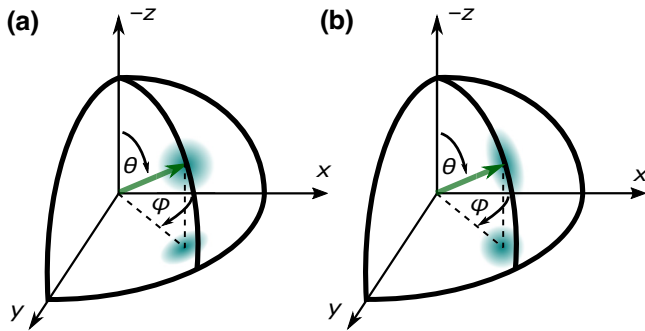


FIG. 1. Spin states represented on the Bloch sphere (southern hemisphere). (a) CSS: the variance contour perpendicular to the mean spin vector (green arrow) exhibits no spin squeezing (circular contour). However, its projection onto the x - y “dipole plane” is squeezed (elliptical), leading to nonclassical radiation (see *dipole-projected squeezing* in Sec. VIA). (b) CRSS exhibits spin squeezing (elliptical contour perpendicular to the mean spin), but no dipole-projected squeezing (circular contour in the x - y plane); hence, it radiates classical light.

case where entanglement between constituent particles is essential for the emergence of a classical response to light.

Counterintuitively, we thus find that a CSS, considered as the classical state of the spin, radiates quantum correlated light, while a CRSS, a quantum entangled spin state, radiates classical light. Hence, for macroscopic spin emitters, there is no clear classical limit: either the spin is classical or the light, but not both. To further explain this result, we establish the connection between quantum fluctuations in spin and light by introducing the concept of *dipole-projected squeezing* (Fig. 1).

Importantly, CRSSs are physical, naturally appearing in superradiance. More generally, however, they form a new family of pure, entangled many-body spin states—the asymptotic eigenstates of \hat{J}_- —and should therefore play a role in collective-spin problems beyond superradiance. We provide a first example to this end, by showing that the CRSS can appear as the ground state of certain Ising many-body spin Hamiltonians.

II. RADIATION FROM DIPOLE EIGENSTATES

The idea that an eigenstate of the lowering operator \hat{J}_- should produce coherent-state radiation is in fact quite generic and can be intuitively understood as follows. Consider a Hermitian dipole operator in the general form $\hat{d}_H = \hat{d} + \hat{d}^\dagger$ coupled to the Hermitian field $\hat{E}_H = \hat{E} + \hat{E}^\dagger$ (with $[\hat{E}, \hat{E}^\dagger] = 1$), both taken dimensionless here. The light-matter interaction Hamiltonian, $\propto \hat{d}_H \hat{E}_H$, within the rotating-wave approximation [27], takes the form

$$\hat{H} \propto \hat{d} \hat{E}^\dagger + \hat{E} \hat{d}^\dagger. \quad (1)$$

If the system is constantly pumped into an eigenstate $|\alpha\rangle$ of \hat{d} with eigenvalue α then we may effectively replace $\hat{d} \rightarrow \alpha$ in Hamiltonian (1) such that the evolution $e^{-\frac{i}{\hbar} \hat{H}t}$ is the displacement operator of the field, generating a coherent state out of an initial vacuum state (see Appendix A). So, an eigenstate of \hat{d} produces coherent-state radiation. Indeed, for a linear dipole, where \hat{d} is a boson lowering operator, $|\alpha\rangle$ is a coherent state of the dipole, which linearly transforms via Eq. (1) to produce a coherent-state field. However, for the nonlinear dipole represented by a spin- j , we first consider the possible existence of eigenstates of $\hat{d} = \hat{J}_-$ and then study their generation and properties.

III. CRSS EXISTS: EIGENSTATE OF \hat{J}_-

Strictly speaking, the operator \hat{J}_- does not have any eigenstates except for the eigenstate $|j, -j\rangle$ with an eigenvalue zero, due to the property $(\hat{J}_-)^{2j+1} = 0$ at finite j ; here we use the common notation $|j, m\rangle$ for the joint eigenstate of the total angular momentum operator $\hat{J}_x^2 + \hat{J}_y^2 + \hat{J}_z^2$ and its z -axis projection \hat{J}_z , with corresponding eigenvalues $j(j+1)$ and $m \in [-j, j]$. However, we show that, for a macroscopic spin, $j \gg 1$, there are states that are approximate eigenstates of \hat{J}_- up to excellent accuracy. We call such states CRSSs. Speaking loosely, we find that in the asymptotic limit $j \rightarrow \infty$, the operator \hat{J}_- has a set of eigenstates with complex eigenvalues α satisfying

$$\hat{J}_- |j, \alpha\rangle = \alpha |j, \alpha\rangle, \quad \alpha = jre^{-i\varphi}, \quad 0 \leq r < 1; r, \varphi \in \mathbb{R}, \quad (2)$$

with $r = 0$ corresponding to the ground state $|j, -j\rangle$. More formally, we define this condition as

$$\lim_{j \rightarrow \infty} \epsilon_j(r) = 0, \quad \epsilon_j(r) \equiv \left\| \hat{J}_- |j, jre^{-i\varphi}\rangle - jre^{-i\varphi} |j, jre^{-i\varphi}\rangle \right\|. \quad (3)$$

Here $\epsilon_j(r)$ is the proximity error of a state $|j, \alpha\rangle$ for being an eigenstate of operator \hat{J}_- with an eigenvalue $\alpha = jre^{-i\varphi}$ ($r < 1$), and we require that this quantity approaches zero for $j \rightarrow \infty$. Importantly, the ratio $\alpha/j = re^{-i\varphi}$ is kept constant while taking the limit $j \rightarrow \infty$. This allows us to account for excitation amplitudes α comparable to j , where nonlinearity becomes significant (beyond the Holstein-Primakoff approximation).

In Appendix B we show a simple way to define a state that satisfies Eq. (3). The result is the following ansatz state and its corresponding error:

$$|j, jre^{-i\varphi}\rangle_{\text{ans}} = \sum_{m=-j}^{m_+} a_m |j, m\rangle, \quad \epsilon_j(r) = jr |a_{m_+}|. \quad (4)$$

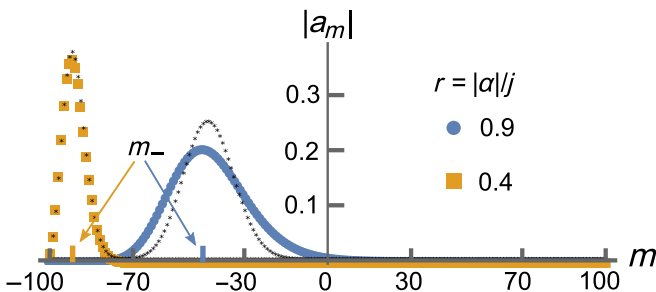


FIG. 2. The CRSS as an approximate eigenstate of the spin- j lowering operator \hat{J}_- with an eigenvalue magnitude $|\alpha| = jr$. For given j and r , the state coefficients $|a_m|$ of the ansatz state, Eqs. (4) and (5), peak at $m = m_-$ and are set to zero for $m > m_+$ ($m_- < m_+ < j$), where $|a_{m\pm}| \rightarrow 0$ as $j \rightarrow \infty$. The resulting Gaussian shape agrees well with the analytical result in Eq. (10). Here $j = 100$ and $r = 0.4, 0.9$ are taken (black stars represent state coefficients of two respective CSSs with matching “magnetization” values $\langle \hat{J}_z \rangle$).

The coefficients a_m are given by

$$a_m = a_{-j} e^{f_m} e^{-i(m+j)\varphi},$$

$$f_m = (m+j) \ln(rj) - \frac{1}{2} \sum_{k=-j}^{m-1} \ln[j(j+1) - k(k+1)], \quad (5)$$

and plotted in Fig. 2. The latter peak at $m = m_-$ and are set to zero for any $m > m_+$, where $m_\pm = \frac{1}{2}[-1 \pm \sqrt{-4(jr)^2 + 4j^2 + 4j + 1}] < j$ (see Appendix B). We see that the last coefficient a_{m+} determines the error $\epsilon_j(r)$ of the ansatz state given in Eq. (4) and must therefore approach zero as $j \rightarrow \infty$ in order to satisfy condition (3). We estimate the error numerically for given j and r , using Eq. (5) for $|a_{m=m_+}|$ and demanding state normalization $|a_{-j}| = [\sum_{m=-j}^{m_+} e^{2f_m}]^{-1/2}$. This is presented in Fig. 3, where we indeed observe that, for $j \gg 1$, the error decreases exponentially with j for any $r < 1$. We also find that at the limit $j \rightarrow \infty$, state (4) coincides with the state that minimizes the error $\epsilon_j(r)$ for fixed j and r (Appendix B 1). We thus conclude that the state (4) is an eigenstate of \hat{J}_- in the sense of Eq. (3), i.e., it is a CRSS to an excellent approximation.

It is instructive to estimate the error from Eq. (4) also analytically, finding, for $j \gg 1$ (see Appendix B),

$$\epsilon_j(r) \approx q e^{-2jg(r)}, \quad g(r) = \operatorname{arctanh}[\sqrt{1-r^2}] - \sqrt{1-r^2}, \quad (6)$$

with the power-law prefactor $q(j, r) = j^{3/4} (r^2 \sqrt{1-r^2} / \pi)^{1/4}$. For $r < 1$, $g(r)$ is positive, so that the error in (6) essentially decays exponentially with j , exhibiting excellent agreement with the numerical results of Fig. 3, and

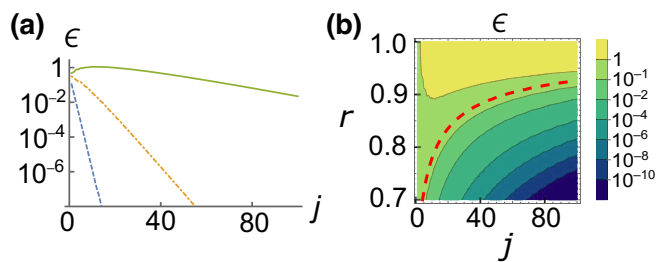


FIG. 3. Proximity error of the CRSS ansatz state given in Eq. (4) [evaluated numerically using Eq. (5)]. (a) Error $\epsilon_j(r)$ versus j for $r = 0.4, 0.7, 0.9$ (dashed, dash-dot, solid lines). Exponential decay is observed for large j , in agreement with Eq. (6). (b) Error $\epsilon_j(r)$ as a function of j and r . The dashed curve marks r_j , defined in Eq. (7a) and calculated using Eq. (6). For given j and $0 < r < r_j$, the state (4) well approximates a CRSS ($\epsilon \ll 1$), as predicted analytically.

yielding the CRSS existence condition $r < 1$ (see also Appendix B 1). The exponent $g(r)$ is a monotonically decreasing function of r , meaning that, for increasing values of r , larger j values are required for the error to still be small, as also seen in Fig. 3. For a given finite $j \gg 1$, we can thus define the range of validity $0 < r < r_j$ in which state (4) is a CRSS to a good approximation, by defining the respective maximal value r_j via

$$\epsilon_j(r = r_j) = \frac{1}{e}, \quad (7a)$$

$$r_j \sim \sqrt{1 - \left(\frac{3}{2j}\right)^{2/3}}, \quad (7b)$$

as marked by the dashed curve in Fig. 3(b). The analytical result (7b) for r_j expresses its asymptotic scaling with j , which is simply obtained by demanding that $2jg(r_j) = 1$ (ignoring the power-law prefactor q for $j \rightarrow \infty$).

IV. CRSS IS PHYSICAL: SUPERRADIANCE

Before we proceed to the analysis of the properties of the CRSS, we first show that it appears in physical problems. The most natural case is that of driven-dissipative superradiance, described by the following scattering problem. Consider a dipole $\hat{d} = \hat{J}_-$ illuminated by a resonant coherent-state light and damped by radiation to a continuum of electromagnetic field modes described by operator \hat{E} . The master equation for the reduced density matrix of the dipole can be derived from Hamiltonian (1) by eliminating the photon modes within a Born-Markov approximation [8,37]:

$$\frac{d\hat{\rho}}{dt} = -\frac{i}{\hbar} (\hat{H}_{\text{nh}} \hat{\rho} - \hat{\rho} \hat{H}_{\text{nh}}^\dagger) + \gamma \hat{J}_- \hat{\rho} \hat{J}_+, \quad (8)$$

$$\hat{H}_{\text{nh}} = \hbar \left(\Delta - i \frac{\gamma}{2} \right) \hat{J}_+ \hat{J}_- - \hbar \left(\Omega \hat{J}_+ + \Omega^* \hat{J}_- \right).$$

Here γ and Δ are the spontaneous emission rate and energy shift, respectively, both induced by the electromagnetic field reservoir, Ω is the amplitude of the incident field, and $\hat{J}_+ = (\hat{J}_-)^{\dagger}$. In the case of superradiance, $\hat{J}_- = \sum_{n=1}^N \hat{\sigma}_n$ describes the collective pseudospin of N two-level atoms with lowering operators $\hat{\sigma}_n = |g\rangle_n\langle e|$ (levels $|g\rangle$ and $|e\rangle$), which are all identically coupled to common field modes described by \hat{E} , as can be realized in an optical cavity [12,13]. The common field reservoir can then mediate correlations between the atoms via the collective decay (γ) and dipole-dipole interaction (Δ). Assuming that all atoms are initially in the ground state, $\prod_n \otimes |g\rangle_n = |N/2, -N/2\rangle$, the spin representation is fixed to $j = N/2$ throughout the dynamics. The steady state of this Lindblad master equation becomes a pure state if and only if it is an eigenstate of both the non-Hermitian Hamiltonian \hat{H}_{nh} and the jump operator \hat{J}_- [38,39]. We showed that the eigenstate (2) of \hat{J}_- exists at the limit $N \rightarrow \infty$ (CRSS) and it is straightforward to verify that it is also an eigenstate of \hat{H}_{nh} if we take

$$\alpha = \frac{\Omega}{\Delta - i\gamma/2}, \quad (9)$$

yielding $d\hat{\rho}/dt = 0$ for $\hat{\rho} = |j, \alpha\rangle\langle j, \alpha|$ with $j = N/2$. This is also seen for a finite $N = 2j \gg 1$ by considering the overlap between the exact steady-state solution of Eq. (8) and the CRSS ansatz (4), whose deviation from unity behaves similarly to the proximity error in Fig. 3 (see Appendix C).

The above considerations establish that, for $N = 2j \gg 1$, the steady state of driven-dissipative superradiance is a CRSS characterized by the amplitude α from Eq. (9). This means that, within the validity range $0 < r < r_j$ from Eq. (7a) wherein the CRSS exists, the properties of a CRSS, a pure state, underlie dissipative superradiance phenomena. As we show below, this allows us to give new analytical predictions and insights into driven-dissipative Dicke superradiance. The expected relevance of the CRSS to physical problems beyond this case is discussed below.

V. CRSS SPIN PROPERTIES

Having established the existence of the CRSS, we now examine the properties of spin variables under a CRSS. These are then related to predictions on physical realizations of a CRSS, such as driven superradiance (discussed here) and an Ising Hamiltonian (Sec. VII below).

A. Mean spin and phase transition

Using Eq. (2), the average dipole $\langle \hat{J}_- \rangle = \langle \hat{J}_x - i\hat{J}_y \rangle$ is trivially given by α . For the “magnetization” \hat{J}_z , we note that the moments of \hat{J}_z can be estimated directly from the distribution $|a_m|^2 \propto e^{2f_m}$ from Eq. (5) and Fig. 2. To this end, we use an integral approximation for f_m and expand it

around its peak at $m = m_-$, finding for $j \gg 1$ that $|a_m|^2$ is well described by a Gaussian,

$$|a_m|^2 \approx \frac{1}{\sqrt{2\pi w^2}} e^{-\frac{(m-m_-)^2}{2w^2}}, \quad m_- \approx -j\sqrt{1-r^2}, \quad (10)$$

of width $w^2 = jr^2/(2\sqrt{1-r^2})$ (see Appendix B 2). This yields the result $\langle \hat{J}_z \rangle \approx m_- \approx -j\sqrt{1-r^2}$, so the average magnetization exhibits a continuous phase transition as a function of $r = |\alpha|/j$. The critical point $r = 1$ coincides with the upper bound $r_j \rightarrow 1$ of the validity region of the CRSS: the error in Eq. (6) changes at $r = 1$ from being exponentially small to oscillatory. Therefore, the magnetization phase transition is a generic property of the CRSS resulting from its existence condition, and should appear in any physical realization of a CRSS.

In particular, the above CRSS predictions underlie the physics of driven-dissipative Dicke superradiance. For example, the mean-field steady-state solution of Eq. (8) is known to exhibit a second-order phase transition for $\langle \hat{J}_z \rangle$, when the driving field $|\Omega|$ crosses the critical point $\Omega_c = (N/4)\sqrt{\gamma^2 + 4\Delta^2}$ [18,34–36,40]. Using the relation to the CRSS from Eq. (9), $r = |\alpha|/j = |\Omega|/\Omega_c$, this exactly matches the magnetization phase transition of the CRSS. The open-system Dicke phase transition thus originates from the existence condition of an underlying pure CRSS state. This connection entails new predictions for superradiance beyond the mean field, as CRSS theory provides the complete probability distribution $|a_m|^2$ of the magnetization [Eqs. (5) and (10)]; e.g., it predicts the scaling of increasingly large fluctuations $\text{Var}[\hat{J}_z] = w^2$ near the critical point $r = |\Omega|/\Omega_c \rightarrow 1$.

For the dipole amplitude, the result $\langle \hat{J}_- \rangle = \alpha \propto \Omega$ agrees with the mean-field solution of superradiance. It implies a linear dependence on the incident field Ω , a result expected for a harmonic oscillator, but less intuitive for our nonlinear spin scatterer. We note that this is valid for very strong fields $r = |\Omega|/\Omega_c \lesssim 1$ well beyond the weakly excited regime $r = |\Omega|/\Omega_c \ll 1$. Such linear-scatter behavior will lead to scattered light that remains in a coherent state, as anticipated above for the CRSS and discussed further below.

B. Spin squeezing

Writing $r = \sin\theta$, we have $\langle \hat{J}_x - i\hat{J}_y \rangle = \langle \hat{J}_- \rangle = \alpha = j \sin\theta e^{-i\varphi}$ and $\langle \hat{J}_z \rangle = -j \cos\theta$, yielding a spin vector $\hat{\mathbf{J}} = (\hat{J}_x, \hat{J}_y, \hat{J}_z)$ whose mean of length $j = N/2$ is directed at an angle θ away from the south pole of the Bloch sphere with an angle φ along the x - y plane [Fig. 1(b)]. This mean spin is equivalent to that of a CSS [Fig. 1(a)]; however, the quantum fluctuations around it are different, as can be characterized by spin squeezing.

The spin-squeezing parameter is defined by $\xi^2 = (2j/|\langle \hat{\mathbf{J}} \rangle|^2) \min_{\phi} \text{Var}[\hat{J}_{\phi}^{\perp}]$, where \hat{J}_{ϕ}^{\perp} is the projection of the spin vector onto an angle ϕ on the plane perpendicular to the direction of the mean spin $\langle \hat{\mathbf{J}} \rangle$ [2,3,23,41]. Here $\xi^2 < 1$ signifies a nonclassical, spin-squeezed state associated with quantum enhanced metrology, whose constituent $N = 2j$ spin-1/2 are pairwise entangled [23,28,29]. The best (minimum) achievable squeezing is bounded by the Heisenberg limit $\xi^2 = 1/N$. Using property (2) of the CRSS, together with $\langle \hat{J}_z \rangle = m_-$, $\text{Var}[\hat{J}_z] = w^2$ from Eq. (10), we find that $\xi^2 = \sqrt{1 - r^2}$ (see Appendix D), so that squeezing grows with r and diminishes in the regime $r \ll 1$ where the CRSS resembles a CSS ($\xi^2 \rightarrow 1$). While this result agrees with that obtained for steady-state superradiance using a mean-field approach (with linearized fluctuations) [20,40], it is strictly exact only for $j \rightarrow \infty$. CRSS theory, however, allows us to extend the analysis to finite-size behavior. For a given finite $j \gg 1$, we recall the validity region $0 < r < r_j$ defined in Eq. (7a). Since minimal $\xi^2 = \sqrt{1 - r^2}$ is achieved for maximal r , then, for a given j , the predictable optimal squeezing for a CRSS is given by

$$\xi_{\min}^2(j) = \sqrt{1 - r_j^2}, \quad (11a)$$

$$\xi_{\min}^2(j) \sim \left(\frac{3}{2j}\right)^{1/3} \propto N^{-1/3}. \quad (11b)$$

Here Eq. (11b) is obtained using r_j from Eq. (7b) and expresses the asymptotic scaling of the CRSS optimal squeezing with $j = N/2 \rightarrow \infty$. The predicted scaling $N^{-1/3}$ does not reach the Heisenberg limit N^{-1} .

We now show how this theory also applies to spin squeezing in superradiance. In Fig. 4(a) we plot ξ^2 as a function of $r = |\Omega|/\Omega_c$ for the exact steady-state solution of Eq. (8) with $j = 25, 100$ (see Appendix D2 for details, in analogy to Refs. [20,34,37]). We observe excellent agreement with the theoretical CRSS result $\sqrt{1 - r^2}$ within the expected validity region $r < r_j$ defined in Eq. (7a). Moreover, for $r > r_j$, ξ^2 begins to grow, setting its minimum at around $r = r_j$. This suggests that the CRSS prediction ξ_{\min}^2 from Eq. (11a) also predicts the best achievable (minimal) spin squeezing in superradiance. This is indeed what is observed in Fig. 4(b), where the minimal ξ^2 of superradiance, obtained with respect to r for different j values as in Fig. 4(a), is plotted as a function of j . Excellent agreement with the CRSS prediction from Eq. (11a) is exhibited. Within this range of j values, a linear fit to the log-log plot yields the scaling $j^{-0.28}$. Extending the range of j values as in the inset of Fig. 4(b), ξ_{\min}^2 from Eq. (11a) scales as $j^{-0.32}$, already in close agreement with the predicted asymptotic scaling $j^{-1/3}$ from Eq. (11b). This finite-size analysis of CRSS theory is useful for predicting spin-squeezing generation in current superradiant systems:

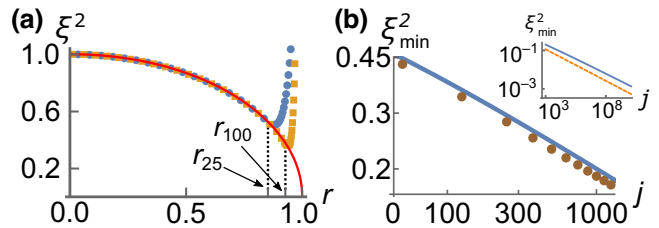


FIG. 4. Spin squeezing ξ^2 in superradiance. (a) Plot of ξ^2 as a function of $r = |\Omega|/\Omega_c$ for the steady state of Eq. (8) with $j = N/2 = 25, 100$ (circles, squares). The optimal (minimum) value ξ_{\min}^2 is seen around $r = r_j$ from Eq. (7a) [calculated using Eq. (6)]. Agreement with CRSS theory (solid line) is observed within the validity region $r < r_j$. (b) Plot of ξ_{\min}^2 defined in (a) as a function of j on a log-log scale (circles). Agreement with CRSS theory (11a) (solid line) is observed. Inset: increasing j , Eq. (11a) scales as $j^{-0.32}$, in close agreement with the asymptotics $j^{-1/3}$ from Eq. (11b) (solid and dashed lines, respectively).

e.g., for $N = 2 \times 10^5$ atoms [13,14], we find an optimal squeezing of ~ 13 dB.

VI. CRSS RADIATION PROPERTIES

After discussing the spin observables in a CRSS, we now turn our attention to the light it radiates. As anticipated above, we see that a CRSS indeed radiates coherent-state light. This, however, leads to a counterintuitive result for superradiance. Since we showed that in steady state the superradiant spin is pumped into a CRSS, then the light emitted in Dicke superradiance is a classical coherent state whose amplitude is linear with the incident driving field. This is identical to scattering by a linear dipole, although the spin- j dipole is highly nonlinear, and nonlinear optical systems typically generate photon interactions and nonclassical light [42]. Notably, this result holds even for very strong fields $|\Omega| \lesssim \Omega_c$ well beyond the “common” linear regime $|\Omega| \ll \Omega_c$ (beyond the Holstein-Primakoff approximation [24]). To illustrate this, consider a generic relation between the field \hat{E} in some detection mode and the radiating dipole \hat{J}_- ,

$$\hat{E}(t) = \hat{E}_0(t) + G\hat{J}_-(t). \quad (12)$$

This relation, written in the Heisenberg picture, can be derived from Eq. (1) within a Born-Markov-type approximation as an input-output relation [26,43], where $\hat{E}_0(t)$ is the freely evolving field excluding interaction with the dipole, and G is a c-number (see Appendix E, e.g., for superradiance in a cavity). In the Schrödinger picture, the solution of Eq. (8) at a steady-state time t is a pure CRSS state of the dipole, $|j, \alpha\rangle_d$, and since the total dipole+field system is closed, then the total state is separable, $|\psi(t)\rangle = |j, \alpha\rangle_d \otimes |\chi\rangle_f$ with some field

state $|\chi\rangle_f$. We now show that this state is a coherent state, i.e., an eigenstate of the (Schrödinger picture) field operator $\hat{E}(0)$. Assuming a vacuum (or coherent) state for the field mode $\hat{E}(0)$ at initial time $t = 0$, and using Eqs. (2) and (12), we find that $\hat{E}(0)|\psi(t)\rangle = G\hat{J}_-(0)|\psi(t)\rangle = G\alpha|\psi(t)\rangle$ (Appendix E). This proves that the steady-state radiation is a coherent state with an amplitude $G\alpha \propto \Omega$ linear in the incident field. Hence, the quantum nonlinear spin system driven to a collective entangled state (CRSS) scatters light as a classical linear system. Importantly, relation (12) also holds for the instantaneous emission at a given time t without resorting to steady-state conditions (Appendix E), leading to the general conclusion that a CRSS radiates coherent-state light regardless of how the CRSS is generated.

Accounting for finite-size effects, the deviation of the radiated field from a coherent state should scale as the CRSS proximity error $\epsilon_j(r)$, decreasing exponentially with $j \gg 1$. We explicitly show this for the variance of the field, whose deviation from that of a coherent state is indeed $\epsilon_j^2(r)$ (Appendix E).

So, we find that a CRSS emits a coherent state. In fact, the converse is also true, as seen from Eq. (12): the system is in an eigenstate of the field \hat{E} (coherent state) provided it is in an eigenstate of \hat{J}_- (CRSS; assuming an initial coherent or vacuum field). Notably, these conclusions rely on relation (12) that, for many atoms, requires their identical couplings to the field mode \hat{E} . Hence, our results do not mean that any coherent-state-like radiation, such as a laser, must originate in a CRSS. For example, in ordinary, nonsuperradiant lasers, relation (12) does not hold within the relevant timescale for emission, due to the much faster individual-atom relaxation [27].

A. Dipole-projected squeezing

Although the CRSS is a quantum correlated spin-squeezed state, we found that it does not radiate quantum correlated squeezed states of light. This calls for a deeper understanding of the general relation between quantum correlations in the spin and the light. To this end, we first observe in Hamiltonian (1) that the field perceives the spin directly only through the dipole operator $\hat{J}_- = \hat{J}_x - i\hat{J}_y$ and hence only through its projection onto the x - y “dipole plane.” This suggests that nonclassical squeezed light is produced only if a similar squeezing exists in the projected x - y spin, hence motivating the distinction between spin squeezing of the total spin and that of the dipole-projected spin. To this end, we define the dipole quadrature $\hat{J}_\phi = (e^{i\phi}\hat{J}_- + e^{-i\phi}\hat{J}_+)/2$, in analogy to the field quadrature $\hat{E}_\phi = e^{i\phi}\hat{E} + e^{-i\phi}\hat{E}^\dagger$. Using Eq. (12) with $[\hat{E}, \hat{E}^\dagger] = 1$ and $[\hat{J}_-, \hat{J}_+] = -2\hat{J}_z$, it follows that the relation between the

variances of these quadratures is

$$\text{Var}[\hat{E}_\phi] = 1 + 4G^2 \left(\text{Var}[\hat{J}_\phi] + \frac{1}{2}\langle\hat{J}_z\rangle \right), \quad (13)$$

where G is taken to be real without loss of generality. Considering the Heisenberg uncertainty $\text{Var}[\hat{J}_\phi]\text{Var}[\hat{J}_{\phi+(\pi/2)}] \geq |\langle\hat{J}_z\rangle|^2/4$, we define the *dipole-projected squeezing* for a quadrature ϕ as $\text{Var}[\hat{J}_\phi] < |\langle\hat{J}_z\rangle|/2$. Then, from Eq. (13) we conclude that, for $\langle\hat{J}_z\rangle < 0$, the emitted light becomes squeezed, i.e., $\text{Var}[\hat{E}_\phi] < 1$, provided that the dipole-projected spin is also squeezed.

For a CRSS, using definition (2), we obtain $\text{Var}[\hat{J}_\phi] = -\langle\hat{J}_z\rangle/2$, so that no dipole squeezing exists and the vacuum noise level is obtained for the light, $\text{Var}[\hat{E}_\phi] = 1$, as expected for a coherent state. This is nicely seen by the geometrical picture in Fig. 1(b): the noise contour perpendicular to the mean spin direction θ, φ presents the spin squeezing of the CRSS with the φ and $\varphi + (\pi/2)$ axes exhibiting increased and reduced variances $(j/2)/\cos\theta$ and $(j/2)\cos\theta$, respectively (also see Appendix D). However, upon projection of the noise contours onto the x - y dipole plane, the φ -axis variance is multiplied by a factor $\cos^2\theta$, so that the noise on both axes is identical and no projected squeezing exists.

For a CSS, the opposite situation occurs, as seen in Fig. 1(a). Whereas the noise contour at the plane perpendicular to the main spin direction is a circle of variance $j/2$ so that no spin squeezing exists [23], the projection onto the x - y dipole plane reduces the noise at the φ direction to $(j/2)\cos^2\theta$, smaller than $|\langle\hat{J}_z\rangle|/2 = (j/2)\cos\theta$. This means that a CSS at the southern Bloch hemisphere, $\langle\hat{J}_z\rangle < 0$, radiates squeezed light. We also verify the latter by a direct calculation of $\text{Var}[\hat{E}_\phi]$ using a CSS [44]. Notably, the intuitive picture provided by the projection of noise contours is a direct consequence of the nonlinearity of the spin system, expressed here through the curvature of the Bloch sphere: The difference between the spin and dipole-projected noise contours, which determines the squeezing, grows with the angle θ and vanishes in the linear, harmonic-oscillator regime $|\alpha|/j = r = \sin\theta \rightarrow 0$.

B. Spin entanglement at the origin of classical light

The above results can be summarized in the following counterintuitive manner: a CSS, which is a noncorrelated many-body spin, emits quantum correlated squeezed light; whereas a CRSS, which is a quantum correlated many-body spin, emits noncorrelated coherent light. The fact that correlations are necessary in a spin system to produce such classical uncorrelated light is nicely seen from a microscopical picture. For dipole-projected squeezing, and hence light squeezing to exist, the phase-dependent variance $\text{Var}[\hat{J}_-] = \langle\hat{J}_-^2\rangle - \langle\hat{J}_-\rangle^2$ also has to exist. Writing this quantity using constituent spin operators $\hat{J}_- =$

$\sum_{n=1}^N \hat{\sigma}_n$ and recalling that $\hat{\sigma}_n^2 = 0$, we have

$$\text{Var}[\hat{J}_-] = - \sum_n \langle \hat{\sigma}_n \rangle^2 + \sum_n \sum_{n \neq m} (\langle \hat{\sigma}_n \hat{\sigma}_m \rangle - \langle \hat{\sigma}_n \rangle \langle \hat{\sigma}_m \rangle). \quad (14)$$

Assuming a coherent drive Ω , where $\langle \hat{\sigma}_n \rangle \neq 0$, and for statistically independent atoms as in a CSS, the second term vanishes such that $\text{Var}[\hat{J}_-] \neq 0$ and light squeezing exists. This typical situation occurs in resonance fluorescence from an ensemble of individual atoms, where the nonlinearity of each two-level atom generates squeezed light [45,46]. For squeezing to vanish, we must have a non-vanishing second term in Eq. (14), namely, nonvanishing correlations between atoms. For a pure state, these correlations imply entanglement, which is exactly the situation in a CRSS where $\text{Var}[\hat{J}_-] = 0$.

VII. CRSS AS A MANY-BODY GROUND STATE

So far, we introduced and discussed the CRSS in the context of radiation. In particular, a CRSS forms the steady state of a dissipative problem of driven superradiance. However, being a pure state, we expect the CRSS to also be realized in Hamiltonian systems. For example, consider the Ising-type Hamiltonian, $\hat{H} = \hat{J}_z - \hat{J}_z^2 - 2\alpha\hat{J}_x$, which includes a transverse field 2α (with $\alpha = jr$ real) and wherein all pairs of spins interact in the same way [47] (all to all, as realized, e.g., in trapped ions [48] and in close analogy to a Lipkin-Meshkov-Glick model [49]). It turns out that the CRSS $|j, \alpha\rangle$ forms the ground state of this Ising model. This is seen by noting that, for a given j representation, \hat{H} can be written (up to a constant) as $\hat{K}^\dagger \hat{K}$, with $\hat{K} = \hat{J}_- - \alpha$. Then, since the eigenvalues of $\hat{K}^\dagger \hat{K}$ must be non-negative and $\hat{K}^\dagger \hat{K}|j, \alpha\rangle = 0$, the CRSS $|j, \alpha\rangle$ forms the ground state of $\hat{K}^\dagger \hat{K}$ and the Ising model \hat{H} . Therefore, all the properties intrinsic to a CRSS found above readily apply here. In particular, the magnetization phase transition at $r = 1$, where a CRSS ceases to exist, means here that the ground state qualitatively changes at the critical point $r = 1$, and that it exhibits spin squeezing for $r < 1$. A detailed study of this system in light of CRSS theory will be the topic of future work. However, this already demonstrates that CRSSs are realized and may offer new predictions in relevant problems beyond radiation.

VIII. DISCUSSION

This study introduces the CRSS as a new class of a macroscopic spin state, possessing rather unusual properties: it is a many-body entangled state that behaves as a macroscopic classical emitter.

These new insights open several important directions. First, since CRSS theory was shown here to describe Dicke superradiance, the above predictions on both photon and

collective-spin observables could be evaluated experimentally in platforms such as cavities [12,13], waveguides [37,50,51], and superconducting resonators [16], with possible applications in spin-squeezing generation for metrology. Moreover, CRSS theory may be conceptually and technically useful for the study of various related collective radiation phenomena. For example, it is interesting to explore the possible role of the CRSS in superradiant lasing [5–7] and whether it can be generalized to account for collective radiation beyond the permutation-symmetric Dicke case [8,52]. This could have important consequences for understanding and exploiting superradiance both in ordered and disordered ensembles [53–65] and for quantum metrology [66–69]. For the latter, the optimal squeezing does not reach the Heisenberg limit; however, it still entails the advantage of a robust dissipative generation of spin squeezing in steady state.

Another direction is the exploration of the very nature of the CRSS as a pure, many-body entangled spin state. The optimal spin squeezing contained in a CRSS exhibits a different scaling, $N^{-1/3}$, than that of spin-squeezed states generated by one- and two-axis twisting Hamiltonians [23,41], with $N^{-2/3}$ and N^{-1} , respectively. It is then interesting to study the existence of a unitary transformation that generates this different class of spin squeezing and its relation to a generating interacting Hamiltonian. Moreover, the Ising model discussed above motivates the study of the relation between the CRSS and quantum phase transitions in Hamiltonian many-body spin systems, providing new insights and predictions into these systems and their connection to dissipative superradiance.

More generally, relying on the finding that a macroscopic spin is perceived as a classical emitter provided that its constituents are quantum entangled, it should be considered if and how this idea extends to other composite quantum systems.

ACKNOWLEDGMENTS

We acknowledge financial support from the Israel Science Foundation (ISF) under Grant No. 2258/20, the ISF and the Directorate for Defense Research and Development (DDR&D) under Grant No. 3491/21, the Center for New Scientists at the Weizmann Institute of Science, the Council for Higher Education (Israel), and QUANTERA (PACE-IN). This research was made possible in part by the historic generosity of the Harold Perlman family.

APPENDIX A: RADIATION FROM A LOWERING OPERATOR EIGENSTATE

Here we show that, for a generic dipole+field system, $\hat{H} = \hbar g(\hat{E}\hat{d}^\dagger + \hat{E}^\dagger\hat{d})$ (coupling constant g), that is pumped into an eigenstate of \hat{d} with an eigenvalue α , one obtains a coherent state of the field \hat{E} , which is equivalent to that

obtained by the replacement $\hat{d} \rightarrow \alpha$ in \hat{H} . We assume that the system is pumped to a state $|\psi(t)\rangle$ that satisfies $\hat{d}(0)|\psi(t)\rangle = \alpha|\psi(t)\rangle$ at any given time t , where $\hat{d}(0)$ is the Scrödinger picture operator. Such a pumping mechanism can be supplied by an external reservoir as in the steady state of Eq. (8) with $\hat{J}_- \leftrightarrow \hat{d}$ and as discussed above for superradiance. We note that

$$\hat{E}(0)|\psi(t)\rangle = \hat{U}(t)\hat{E}(t)|\psi(0)\rangle, \quad \hat{U}(t) = e^{-\frac{i}{\hbar}\hat{H}t}, \quad (\text{A1})$$

where $|\psi(t)\rangle = \hat{U}(t)|\psi(0)\rangle$ and $\hat{E}(t) = \hat{U}^\dagger(t)\hat{E}(0)\hat{U}(t)$ is the Heisenberg picture operator, formally obtained from the Heisenberg equations as

$$\hat{E}(t) = \hat{E}(0) - ig \int_0^t dt' \hat{d}(t'). \quad (\text{A2})$$

Inserting Eq. (A2) into Eq. (A1), assuming an initial vacuum state of the field, $\hat{E}(0)|\psi(0)\rangle = 0$, and using $\hat{d}(t') = \hat{U}^\dagger(t')\hat{d}(0)\hat{U}(t')$, we obtain

$$\begin{aligned} \hat{E}(0)|\psi(t)\rangle &= -ig\hat{U}(t) \int_0^t dt' \hat{U}^\dagger(t')\hat{d}(0)|\psi(t')\rangle \\ &= -ig\alpha\hat{U}(t) \int_0^t dt' \hat{U}^\dagger(t')|\psi(t')\rangle \\ &= -ig\alpha t|\psi(t)\rangle, \end{aligned} \quad (\text{A3})$$

where the pumping assumption, $\hat{d}(0)|\psi(t')\rangle = \alpha|\psi(t')\rangle$, was used in the second equality. Equation (A3) then shows that $|\psi(t)\rangle$ is a coherent state with an amplitude $-ig\alpha t$, just as one would get from the displacement operator $\hat{U}(t) = e^{-\frac{i}{\hbar}\hat{H}t}$ formed by setting $\hat{d} \rightarrow \alpha$ in \hat{H} .

APPENDIX B: THE CRSS ANSATZ OF EQ. (4)

We present a simple approach for finding states that satisfy Eq. (3). Assuming that Eq. (2) can be solved, we insert into this equation the general state $\sum_{m=-j}^j a_m|j, m\rangle$ and obtain the recursion relation

$$a_{m+1} = \frac{\alpha}{\sqrt{j(j+1) - m(m+1)}} a_m, \quad -j \leq m \leq j-1, \quad (\text{B1})$$

together with $a_j = 0$. These two conditions result in a contradiction for any $|\alpha| > 0$ unless a_j tends to zero in the required limit $j \rightarrow \infty$. Using the solution for the recursion relation (B1), given in Eq. (5), we plot $|a_m/a_{-j}|$ as a function of m in Fig. 5, and observe that, depending on r , a_j does not always tend to zero as required. We find analytically and numerically that, as $j \rightarrow \infty$, $a_j \rightarrow 0$ only for $r < 0.804 \dots$ [44]. To satisfy Eq. (3) in the full domain $0 < r < 1$, we use the following observation: for

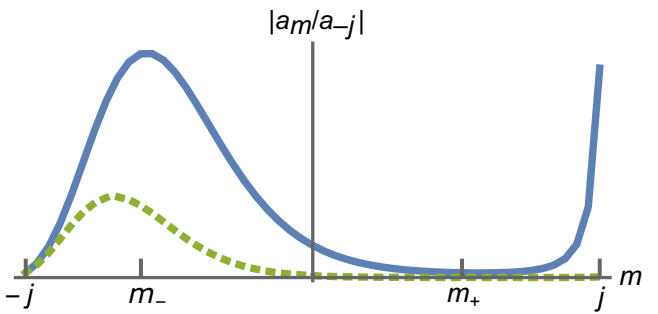


FIG. 5. State coefficients $|a_m/a_{-j}|$ from Eq. (5) with $j = 25$ ($m = -j, \dots, j$). For $r = 0.75$ (dashed line), a_j approximately vanishes, whereas for $r = 0.84$ (solid line), it does not. For the latter, the maximum and minimum points m_\pm are marked. In the CRSS ansatz (4), all coefficients $m > m_+$ are set to zero, and condition (3) is satisfied for all $r < 1$.

a truncated state $|\psi_s\rangle = \sum_{m=-j}^s a_m|j, m\rangle$ with $s < j$, we find that the proximity error is proportional to the last coefficient $\|\hat{J}_-|\psi_s\rangle - \alpha|\psi_s\rangle\| = |\alpha a_s|$. Using Eq. (B1), we can identify the regions for which $|a_m|$ is increasing or decreasing as a function of m , finding the maximum (m_-) and minimum (m_+) points as the roots of the quadratic equation $|\alpha|^2 = j(j+1) - m(m+1)$ (rounded to integers); see Fig. 5. For the minimal proximity error $\propto |\alpha a_s|$, we thus choose to truncate at $s = m_+$, defining our ansatz eigenstate and resulting error as those from Eq. (4). For the analytical estimation of the error from Eq. (4), we write $|a_{m+}| = e^{f_{m+}-f_{m-}}|a_{m-}|$, approximate $f_{m\pm}$ by converting the sum to an integral in Eq. (5) [see Eq. (B2) below], and estimate $|a_{m-}|$ using Eq. (10) above, obtaining for $j \gg 1$ the error from Eq. (6).

1. Minimization of the proximity error

We showed that the error $\epsilon_j(r)$ of the state $|j, \alpha\rangle_{\text{ans}}$ from Eq. (4) goes to zero exponentially. Here we show that it also does so in the optimal way. We define the state $|\alpha, j\rangle_{\text{min}}$ that minimizes $\epsilon_j(r)$ in Eq. (3), while keeping j and α fixed. Such a state would then form an optimal definition of a CRSS at finite j , and we now show that $|j, \alpha\rangle_{\text{ans}}$ indeed becomes equivalent to the optimal state $|\alpha, j\rangle_{\text{min}}$ for $j \gg 1$. Writing the error for a state $|\psi\rangle$ as $\epsilon_\psi = \|\hat{K}|\psi\rangle\|$ with $\hat{K} = \hat{J}_- - \alpha$, $|\alpha, j\rangle_{\text{min}}$ is given by the state $|\psi\rangle$ that minimizes $\epsilon_\psi^2 = \langle\psi|\hat{K}^\dagger\hat{K}|\psi\rangle$. Since the lower bound of this quantity is the smallest eigenvalue of $\hat{K}^\dagger\hat{K}$, its corresponding eigenstate is in fact the state $|\alpha, j\rangle_{\text{min}}$, and can be readily evaluated numerically for given j and α . Figure 6(a) compares the two definitions $|j, \alpha\rangle_{\text{ans}}$ and $|j, \alpha\rangle_{\text{min}}$, by displaying the infidelity $1 - |\langle\text{ans}|j, \alpha|j, \alpha\rangle_{\text{min}}|$. It is seen that this infidelity decreases exponentially with j , indicating that the two definitions coalesce in the relevant limit $j \rightarrow \infty$. Therefore, while, for a finite j , one may in principle find other ansatz states of a CRSS

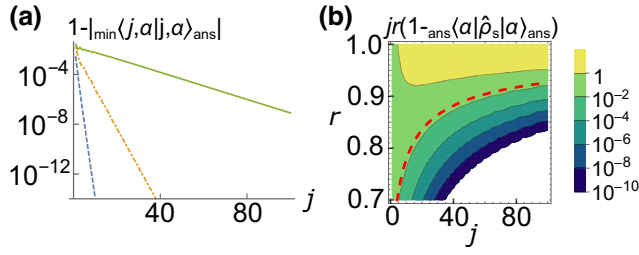


FIG. 6. (a) The infidelity between the state $|j, \alpha\rangle_{\min}$ that minimizes the proximity error and the CRSS ansatz $|j, \alpha\rangle_{\text{ans}}$ decays exponentially with j , so that the states coalesce for $j \rightarrow \infty$ ($r = 0.4, 0.7, 0.9$; dashed, dash-dot, solid lines). (b) The infidelity between the exact steady state $\hat{\rho}_s$ of Eq. (8) and the CRSS ansatz behaves similar to the proximity error in Fig. 3(b), as expected. Therefore, $\hat{\rho}_s \approx |j, \alpha\rangle_{\text{ans}}\langle j, \alpha|$ forms an excellent approximation at any finite $j \gg 1$ for $0 < r < r_j$ (dashed curve marks r_j and the white parts represent values too small for our numerical evaluation).

different from $|j, \alpha\rangle_{\text{ans}}$ of Eq. (4), the latter exponentially approaches the optimal CRSS and hence serves as an excellent approximation of a CRSS for any practical purpose. This also means that the CRSS existence condition and validity range $r < r_j \rightarrow 1$ found from $|j, \alpha\rangle_{\text{ans}}$ forms a general result for the CRSS. We demonstrate this by plotting in Fig. 7 the minimal proximity error, i.e., that evaluated from the optimal state $|\alpha, j\rangle_{\min}$, observing its monotonic increase with j for $r > 1$, as opposed to the exponential decrease for $r < 1$.

2. Expansion of the distribution $|a_m|^2$

From Eq. (5) we have $|a_m|^2 \propto e^{2f_m}$. Approximating the sum in $f_m = f(m)$ by an integral, we obtain

$$\begin{aligned} f(m) = & -\frac{1}{2}j \ln \left[\frac{4j^2(j+m)}{j-m+1} \right] + (j+m)[\ln(jr) + 1] \\ & -\frac{1}{2}m \ln[j(j+1) - m(m-1)] \\ & + \frac{1}{2} \ln(j-m+1) - 1. \end{aligned} \quad (\text{B2})$$

Expanding $f(m)$ around the peak $m = m_-$, we find that

$$\begin{aligned} f(m) \approx & A_0 - A_2(m - m_-)^2 \\ & + A_3(m - m_-)^3 + A_4(m - m_-)^4 \end{aligned} \quad (\text{B3})$$

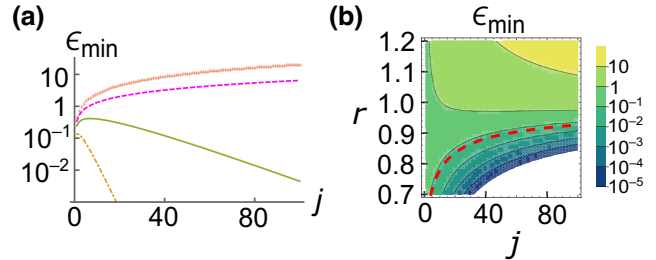


FIG. 7. Minimal proximity error, ϵ_{\min} , of the minimizing state $|j, \alpha\rangle_{\min}$. (a) For $r < 1$, this error decays exponentially with j , as in Fig. 3(a) ($r = 0.7, 0.9$; dash-dot, solid lines), whereas for $r > 1$, it grows with j ($r = 1.05, 1.2$; dashed line, crosses). (b) Plot of ϵ_{\min} as a function of both j and r exhibits low values within the validity region $r < r_j$ (dashed curve). Plots (a) and (b) thus directly validate the generality of the error and existence condition $r < r_j < 1$ derived using the CRSS ansatz state $|j, \alpha\rangle_{\text{ans}}$.

with the expansion coefficients, for $j \gg 1$,

$$\begin{aligned} A_2(j, r) & \approx \frac{\sqrt{1-r^2}}{2r^2} \frac{1}{j}, \\ A_3(j, r) & \approx \left(\frac{1}{3r^4} - \frac{1}{6r^2} \right) \frac{1}{j^2}, \\ A_4(j, r) & \approx \frac{\sqrt{1-r^2}}{3r^4} \left(\frac{1}{4} - \frac{1}{r^2} \right) \frac{1}{j^3}, \end{aligned}$$

and where A_0 is of no importance here. For a Gaussian approximation to be valid, only the A_2 term should be significant. This term implies a distribution width of order $w = [jr^2/(2\sqrt{1-r^2})]^{1/2} \propto \sqrt{j}$, so that the terms $A_n \propto j^{-n+1}$ for $n > 2$ are negligible if $A_n w^n \ll 1$. It can be verified that this is indeed the case if we demand $\sqrt{1-r^2} j^{1/3} \gg 1$. This is equivalent to the CRSS validity condition $r < r_j$ with the asymptotic r_j from Eq. (7b). In this case, we obtain a Gaussian distribution and, demanding normalization, we arrive at Eq. (10).

APPENDIX C: SUPERRADIANCE AT FINITE j

For a finite $j \gg 1$, the state $|j, \alpha\rangle_{\text{ans}}$ from Eq. (4) is a CRSS to an excellent approximation in the range $r < r_j$ with r_j from Eq. (7a). We thus expect that, within this range, $|j, \alpha\rangle_{\text{ans}}$ also well approximates the steady state of the superradiance master equation (8). For the case $\Delta = 0$, the latter is given by $\hat{\rho}_s \propto [(\hat{J}_- - \alpha)^\dagger (\hat{J}_- - \alpha)]^{-1}$ [31,32] and can be readily evaluated numerically within the basis states $|j, m\rangle$ for given j and $r = |\Omega|/\Omega_c$. In Fig. 6(b) we plot the infidelity between the state (4) and the exact steady state $\hat{\rho}_s$, $jr(1 - \text{ans}\langle j, \alpha | \hat{\rho}_s | j, \alpha \rangle_{\text{ans}})$, observing a similar dependence on j and r as that of the CRSS proximity error in Fig. 3(b). In particular, the curve r_j (dashed line) indeed overlaps with an infidelity contour beyond which state

$|j, \alpha\rangle_{\text{ans}}$ well approximates $\hat{\rho}_s$. The normalization factor $j r$ in the above infidelity definition is analogous to that in the proximity error in Eqs. (3) and (4). This error (or infidelity) definition means that an error of order < 1 leads to values of typical spin correlators (e.g., $\langle \hat{J}_-^2 \rangle$) that agree with their CRSS values ($\langle \hat{J}_- \rangle^2$) up to a correction smaller by a factor of $\sim 1/|\alpha| = 1/(jr)$ (similar to a mean-field assumption).

APPENDIX D: SPIN SQUEEZING

1. CRSS spin-squeezing calculation

For the spin squeezing, one has to calculate the variance of the spin operator \hat{J}_ϕ^\perp that is projected to the plane perpendicular to the mean spin vector (MSV). The latter defines the angles θ and φ from the main text, and hence the corresponding rotated coordinate system in which the MSV points to a rotated z' axis. Within this rotated coordinate system, the lowering spin operator $\hat{J}'_- = \hat{J}'_x - i\hat{J}'_y$ (with \hat{J}'_i the spin projection onto the rotated $i \in \{x', y'\}$ axis) is given in terms of the original spin operators via the transformation

$$\hat{J}'_- = e^{i\varphi} \frac{\cos \theta + 1}{2} \hat{J}_- + e^{-i\varphi} \frac{\cos \theta - 1}{2} \hat{J}_+ - \sin \theta \hat{J}_z, \quad (\text{D1})$$

recalling that $\sin \theta = r$. A general Hermitian spin operator on the plane perpendicular to the MSV is then given by $\hat{J}_\phi^\perp = (e^{i\phi} \hat{J}'_- + e^{-i\phi} \hat{J}'_+)/2$. Calculating the variance of this operator involves various first- and second-order moments of \hat{J}_- , \hat{J}_+ , and \hat{J}_z , all of which can be evaluated using the CRSS property (2), the moments of \hat{J}_z from Eq. (10), and the SU(2) commutation relations $[\hat{J}_-, \hat{J}_+] = -2\hat{J}_z$ and $[\hat{J}_-, \hat{J}_z] = \hat{J}_-$. Recalling the mean spin length $|\langle \hat{\mathbf{J}} \rangle| = j$ in a CRSS, we finally have

$$\xi_\phi^2 = \frac{2j \text{Var}[\hat{J}_\phi^\perp]}{|\langle \hat{\mathbf{J}} \rangle|^2} = \cos[2(\phi - \varphi)] \frac{1 - c^2}{2c} + \frac{1 + c^2}{2c} \quad (\text{D2})$$

with $c = \sqrt{1 - r^2}$. The minimal noise is obtained for $\phi = \varphi + \pi/2$, yielding the spin squeezing $\xi^2 = \xi_{\varphi+\pi/2}^2 = c = \sqrt{1 - r^2} = \cos \theta < 1$, whereas the conjugate quadrature $\phi = \varphi$ exhibits antisqueezing, $\xi_\varphi^2 = 1/\cos \theta > 1$. This is illustrated in Fig. 1(b).

2. Steady-state superradiance: direct calculation

We use the exact steady-state density matrix solution of Eq. (8), $\hat{\rho}_s \propto [(\hat{J}_- - \alpha)^\dagger (\hat{J}_- - \alpha)]^{-1}$ (see Appendix C and Refs. [31,32]) to numerically calculate any expectation value of the spin operators. In particular, for the spin-squeezing parameter in Fig. 4, $\xi^2 = (2j / |\langle \hat{\mathbf{J}} \rangle|^2) \min_\phi \text{Var}[\hat{J}_\phi^\perp]$, we first find the expectation values of $\langle \hat{\mathbf{J}} \rangle$. Then, we find a rotation matrix R that transforms

$\langle \hat{\mathbf{J}} \rangle$ to the direction pointing at the $-z$ direction, i.e.,

$$R \cdot \frac{\langle \hat{\mathbf{J}} \rangle}{|\langle \hat{\mathbf{J}} \rangle|} = \begin{bmatrix} 0 \\ 0 \\ -1 \end{bmatrix}. \quad (\text{D3})$$

The plane perpendicular to the mean spin $\langle \hat{\mathbf{J}} \rangle$ is spanned by the two vectors $\mathbf{n}_x = R^{-1} \cdot (1, 0, 0)^T$, $\mathbf{n}_y = R^{-1} \cdot (0, 1, 0)^T$. Therefore, $\hat{J}_\phi^\perp = (\cos(\phi)\mathbf{n}_x + \sin(\phi)\mathbf{n}_y) \cdot \hat{\mathbf{J}}$, and we minimize $\text{Var}[\hat{J}_\phi^\perp]$ over the direction ϕ , to obtain the spin-squeezing parameter.

APPENDIX E: THE SCATTERED FIELD

1. Relation between field and dipole variables

The relation (12) between the output field and the radiating dipole can be generally obtained in the Heisenberg picture. One typical case is that of a dipole damped by a continuum of photon modes described by an operator \hat{E} in Eq. (1), in equivalence to the master equation (8) and in analogy to input-output theory [26] (where G is often related to the photon Green function [43,70]). For example, consider superradiance in a leaky cavity, where the atoms are situated at positions where they are identically coupled to the cavity mode \hat{a} and driven by a laser Ω . The Hamiltonian is given by

$$\hat{H} = -\hbar \delta_a \hat{J}_z - \hbar \delta_c \hat{a}^\dagger \hat{a} + \hbar \left[(g^* \hat{a}^\dagger + \Omega^*) \hat{J}_- + \text{H.c.} \right], \quad (\text{E1})$$

where δ_a and δ_c are the detunings of the dipole and the cavity from the driving-laser frequency. Considering the damping of the cavity to the outside modes through its leaky mirrors at a rate κ , and exploiting the separation of time scales $\kappa \gg g$, we formally solve the Heisenberg-Langevin equation for \hat{a} at $t \gg 1/\kappa$, obtaining

$$g\hat{a}(t) = \left(\Delta - i\frac{\gamma}{2} \right) \hat{J}_-(t) + \hat{f}(t), \quad \Delta - i\frac{\gamma}{2} = \frac{|g|^2}{\delta_c + i\kappa/2}. \quad (\text{E2})$$

Here $\hat{f}(t)$ is a Langevin noise due to the freely evolving (vacuum) field of the modes to which the cavity is damped, satisfying $\hat{f}(t)|\psi(0)\rangle = 0$, where the initial state $|\psi(0)\rangle$ is in the field's vacuum. We identify that Eq. (E2) is equivalent to Eq. (12) with the “detection mode” \hat{E} being the cavity mode. A similar relation can be obtained between the dipole and the outside field modes.

A simpler case wherein a relation of type (12) holds is that of the instantaneous field emitted at a given time $t \equiv 0$. This is seen by the general solution of Eq. (A2) for a dipole $\hat{d} = \hat{J}_-$ and a short evolution time τ after $t = 0$, given by $\hat{E}(\tau) \approx \hat{E}(0) - ig\tau \hat{J}_-(0)$.

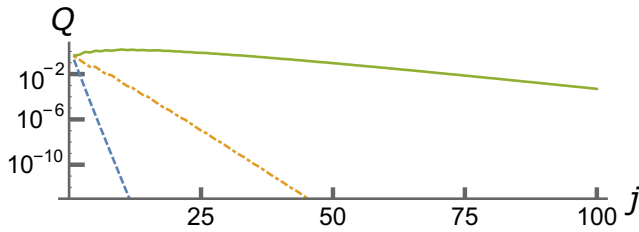


FIG. 8. Deviation of the variance of the radiated field from that of a coherent state, $Q = Q_{\phi=0}$ from Eq. (E3), calculated numerically as a function of j using the CRSS ansatz state from Eq. (4) ($r = 0.4, 0.7, 0.9$; dashed, dash-dot, solid lines). Exponential decay with j is observed, and agreement with the analytical result $\epsilon_j^2(r)$ of Eq. (6) is verified.

2. Coherent state and finite-size corrections

Once relation (12) is established, and using $\hat{E}_0(t)|\psi(0)\rangle = 0$ for the freely evolving vacuum, a similar algebra to that of Eq. (A3) leads to $\hat{E}(0)|\psi(t)\rangle = \hat{G}\hat{U}(t)\hat{J}_-(t)|\psi(0)\rangle = G\hat{J}_-(0)|\psi(t)\rangle = G\alpha|\psi(t)\rangle$, thus showing that the radiated field is a coherent state. Here we used the fact that $|\psi(t)\rangle$ is a CRSS and is hence an eigenstate of \hat{J}_- ; however, for a finite j , this statement is precise only up to the proximity error $\epsilon_j(r)$. Therefore, the deviation of the radiated light from a coherent state at finite j should directly follow the deviation $\epsilon_j(r)$ of the CRSS from being an eigenstate of \hat{J}_- . We now demonstrate this for the variance of the radiated field. We rewrite the variance of the field quadrature \hat{E}_ϕ from Eq. (13) as

$$\begin{aligned} \text{Var}[\hat{E}_\phi] &= 1 + 2|G|^2Q_\phi, \\ Q_\phi &= \langle \hat{K}^\dagger \hat{K} \rangle - |\langle \hat{K} \rangle|^2 + \cos(2\phi)|\langle \hat{K}^2 \rangle - \langle \hat{K} \rangle^2|, \end{aligned} \quad (\text{E3})$$

where $\hat{K} = \hat{J}_- - \alpha$, and taking $G^2(\langle \hat{K}^2 \rangle - \langle \hat{K} \rangle^2)$ real without loss of generality. The quantity Q_ϕ measures the deviation of the field variance from the coherent-state result 1. In order to calculate Q_ϕ , we evaluate the correlators of \hat{K} by averaging with the CRSS ansatz $|j, \alpha\rangle_{\text{ans}}$ from Eq. (4), finding that $\langle \hat{K}^\dagger \hat{K} \rangle = \epsilon_j^2(r)$, $\langle \hat{K} \rangle = \epsilon_j^2(r)/\alpha^*$, and $\langle \hat{K}^2 \rangle = \mathcal{O}(\langle \hat{K} \rangle)$. Recalling that $\alpha \propto j \gg 1$ and that $\epsilon_j(r)$ decays exponentially with j , we find to leading order that only the first term in Eq. (E3) matters, so that the deviation Q_ϕ is independent of ϕ and indeed given by the CRSS proximity error, $Q_\phi \approx \epsilon_j^2(r)$. This is seen in Fig. 8, where we plot Q_ϕ from Eq. (E3) obtained numerically using the exact coefficients a_m of the ansatz state from Eq. (5). We verify that the numerical curves indeed agree with $\epsilon_j^2(r)$ given by the analytical expression in Eq. (6).

- [2] D. J. Wineland, J. J. Bollinger, W. M. Itano, F. L. Moore, and D. J. Heinzen, Spin squeezing and reduced quantum noise in spectroscopy, *Phys. Rev. A* **46**, R6797 (1992).
- [3] D. J. Wineland, J. J. Bollinger, W. M. Itano, and D. J. Heinzen, Squeezed atomic states and projection noise in spectroscopy, *Phys. Rev. A* **50**, 67 (1994).
- [4] V. Paulisch, M. Perarnau-Llobet, A. González-Tudela, and J. I. Cirac, Quantum metrology with one-dimensional superradiant photonic states, *Phys. Rev. A* **99**, 043807 (2019).
- [5] F. Haake, M. I. Kolobov, C. Seeger, C. Fabre, E. Giacobino, and S. Reynaud, Quantum noise reduction in stationary superradiance, *Phys. Rev. A* **54**, 1625 (1996).
- [6] D. Meiser, J. Ye, D. Carlson, and M. Holland, Prospects for a millihertz-linewidth laser, *Phys. Rev. Lett.* **102**, 163601 (2009).
- [7] J. G. Bohnet, Z. Chen, J. M. Weiner, D. Meiser, M. J. Holland, and J. K. Thompson, A steady-state superradiant laser with less than one intracavity photon, *Nature* **484**, 78 (2012).
- [8] M. Gross and S. Haroche, Superradiance: An essay on the theory of collective spontaneous emission, *Phys. Rep.* **93**, 301 (1982).
- [9] R. H. Dicke, Coherence in spontaneous radiation processes, *Phys. Rev.* **93**, 99 (1954).
- [10] L. Mandel and E. Wolf, *Optical Coherence and Quantum Optics* (Cambridge University Press, Cambridge, UK, 1995).
- [11] P. Kirton, M. M. Roses, J. Keeling, and E. G. Dalla Torre, Introduction to the Dicke model: from equilibrium to nonequilibrium, and vice versa, *Adv. Quantum Technol.* **2**, 1800043 (2019).
- [12] Y. Kaluzny, P. Goy, M. Gross, J. Raimond, and S. Haroche, Observation of self-induced Rabi oscillations in two-level atoms excited inside a resonant cavity: The ringing regime of superradiance, *Phys. Rev. Lett.* **51**, 1175 (1983).
- [13] M. A. Norcia, M. N. Winchester, J. R. Cline, and J. K. Thompson, Superradiance on the millihertz linewidth strontium clock transition, *Sci. Adv.* **2**, e1601231 (2016).
- [14] M. A. Norcia, J. R. Cline, J. A. Muniz, J. M. Robinson, R. B. Hutson, A. Goban, G. E. Marti, J. Ye, and J. K. Thompson, Frequency measurements of superradiance from the strontium clock transition, *Phys. Rev. X* **8**, 021036 (2018).
- [15] D. D. Grimes, S. L. Coy, T. J. Barnum, Y. Zhou, S. F. Yelin, and R. W. Field, Direct single-shot observation of millimeter-wave superradiance in Rydberg-Rydberg transitions, *Phys. Rev. A* **95**, 043818 (2017).
- [16] A. Angerer, K. Streltsov, T. Astner, S. Putz, H. Sumiya, S. Onoda, J. Isoya, W. J. Munro, K. Nemoto, and J. Schmiedmayer, *et al.*, Superradiant emission from colour centres in diamond, *Nat. Phys.* **14**, 1168 (2018).
- [17] Z. Wang, T. Jaako, P. Kirton, and P. Rabl, Supercorrelated radiance in nonlinear photonic waveguides, *Phys. Rev. Lett.* **124**, 213601 (2020).
- [18] P. Drummond and H. Carmichael, Volterra cycles and the cooperative fluorescence critical point, *Opt. Commun.* **27**, 160 (1978).
- [19] E. M. Kessler, G. Giedke, A. Imamoglu, S. F. Yelin, M. D. Lukin, and J. I. Cirac, Dissipative phase transition in a central spin system, *Phys. Rev. A* **86**, 012116 (2012).

- [20] T. E. Lee, C.-K. Chan, and S. F. Yelin, Dissipative phase transitions: Independent versus collective decay and spin squeezing, *Phys. Rev. A* **90**, 052109 (2014).
- [21] J. Hannukainen and J. Larson, Dissipation-driven quantum phase transitions and symmetry breaking, *Phys. Rev. A* **98**, 042113 (2018).
- [22] F. T. Arecchi, E. Courtens, R. Gilmore, and H. Thomas, Atomic coherent states in quantum optics, *Phys. Rev. A* **6**, 2211 (1972).
- [23] J. Ma, X. Wang, C. Sun, and F. Nori, Quantum spin squeezing, *Phys. Rep.* **509**, 89 (2011).
- [24] A. Auerbach, *Interacting Electrons and Quantum Magnetism* (Springer Science & Business Media, New York, NY, 2012).
- [25] J. P. Dowling, G. S. Agarwal, and W. P. Schleich, Wigner distribution of a general angular-momentum state: Applications to a collection of two-level atoms, *Phys. Rev. A* **49**, 4101 (1994).
- [26] D. F. Walls and G. J. Milburn, *Quantum Optics* (Springer Science & Business Media, Springer Berlin, Heidelberg, 2007).
- [27] M. Scully and M. Zubairy, *Quantum Optics* (Cambridge University Press, Cambridge, UK, 1997).
- [28] J. Korbicz, J. I. Cirac, and M. Lewenstein, Spin squeezing inequalities and entanglement of N qubit states, *Phys. Rev. Lett.* **95**, 120502 (2005).
- [29] A. Sørensen, L.-M. Duan, J. I. Cirac, and P. Zoller, Many-particle entanglement with Bose-Einstein condensates, *Nature* **409**, 63 (2001).
- [30] P. D. Drummond, Observables and moments of cooperative resonance fluorescence, *Phys. Rev. A* **22**, 1179 (1980).
- [31] H. Carmichael, Analytical and numerical results for the steady state in cooperative resonance fluorescence, *J. Phys. B: At., Mol. Phys. (1968-1987)* **13**, 3551 (1980).
- [32] R. Puri and S. Lawande, Exact steady-state density operator for a collective atomic system in an external field, *Phys. Lett. A* **72**, 200 (1979).
- [33] J. Huber, P. Kirton, and P. Rabl, Phase-space methods for simulating the dissipative many-body dynamics of collective spin systems, *SciPost Phys.* **10**, 045 (2021).
- [34] D. Barberena, R. J. Lewis-Swan, J. K. Thompson, and A. M. Rey, Driven-dissipative quantum dynamics in ultra-long-lived dipoles in an optical cavity, *Phys. Rev. A* **99**, 053411 (2019).
- [35] K. Tucker, D. Barberena, R. J. Lewis-Swan, J. K. Thompson, J. G. Restrepo, and A. M. Rey, Facilitating spin squeezing generated by collective dynamics with single-particle decoherence, *Phys. Rev. A* **102**, 051701 (2020).
- [36] C. S. Muñoz, B. Buća, J. Tindall, A. González-Tudela, D. Jaksch, and D. Porras, Symmetries and conservation laws in quantum trajectories: Dissipative freezing, *Phys. Rev. A* **100**, 042113 (2019).
- [37] A. González-Tudela and D. Porras, Mesoscopic entanglement induced by spontaneous emission in solid-state quantum optics, *Phys. Rev. Lett.* **110**, 080502 (2013).
- [38] N. Yamamoto, Parametrization of the feedback Hamiltonian realizing a pure steady state, *Phys. Rev. A* **72**, 024104 (2005).
- [39] B. Kraus, H. P. Büchler, S. Diehl, A. Kantian, A. Micheli, and P. Zoller, Preparation of entangled states by quantum Markov processes, *Phys. Rev. A* **78**, 042307 (2008).
- [40] O. Somech, Y. Shimshi, and E. Shahmoon, Heisenberg-Langevin approach to driven superradiance, *Phys. Rev. A* **108**, 023725 (2023).
- [41] M. Kitagawa and M. Ueda, Squeezed spin states, *Phys. Rev. A* **47**, 5138 (1993).
- [42] D. E. Chang, V. Vuletić, and M. D. Lukin, Quantum nonlinear optics—photon by photon, *Nat. Photonics* **8**, 685 (2014).
- [43] H. T. Dung, L. Knöll, and D.-G. Welsch, Resonant dipole-dipole interaction in the presence of dispersing and absorbing surroundings, *Phys. Rev. A* **66**, 063810 (2002).
- [44] See Supplemental Material at <http://link.aps.org/supplemental/10.1103/PRXQuantum.5.010349> containing more details in the following subjects: (1) eigenstates of \hat{J}_- without truncation; (2) radiated light from a CSS: direct calculation.
- [45] D. F. Walls and P. Zoller, Reduced quantum fluctuations in resonance fluorescence, *Phys. Rev. Lett.* **47**, 709 (1981).
- [46] W. Vogel and D. G. Welsch, Squeezing pattern in resonance fluorescence from a regular n -atom system, *Phys. Rev. Lett.* **54**, 1802 (1985).
- [47] A. Das, K. Sengupta, D. Sen, and B. K. Chakrabarti, Infinite-range Ising ferromagnet in a time-dependent transverse magnetic field: Quench and ac dynamics near the quantum critical point, *Phys. Rev. B* **74**, 144423 (2006).
- [48] C. Monroe, W. C. Campbell, L.-M. Duan, Z.-X. Gong, A. V. Gorshkov, P. W. Hess, R. Islam, K. Kim, N. M. Linke, and G. Pagano, *et al.*, Programmable quantum simulations of spin systems with trapped ions, *Rev. Mod. Phys.* **93**, 025001 (2021).
- [49] H. J. Lipkin, N. Meshkov, and A. Glick, Validity of many-body approximation methods for a solvable model: (I). Exact solutions and perturbation theory, *Nucl. Phys.* **62**, 188 (1965).
- [50] A. Goban, C.-L. Hung, J. Hood, S.-P. Yu, J. Muniz, O. Painter, and H. Kimble, Superradiance for atoms trapped along a photonic crystal waveguide, *Phys. Rev. Lett.* **115**, 063601 (2015).
- [51] D. Chang, J. Douglas, A. González-Tudela, C.-L. Hung, and H. Kimble, Colloquium: Quantum matter built from nanoscopic lattices of atoms and photons, *Rev. Mod. Phys.* **90**, 031002 (2018).
- [52] G.-D. Lin and S. F. Yelin, in *Advances in Atomic, Molecular, and Optical Physics*, Vol. 61 (Elsevier, 2012), p. 295.
- [53] E. Shahmoon, D. S. Wild, M. D. Lukin, and S. F. Yelin, Cooperative resonances in light scattering from two-dimensional atomic arrays, *Phys. Rev. Lett.* **118**, 113601 (2017).
- [54] J. Rui, D. Wei, A. Rubio-Abadal, S. Hollerith, J. Zeiher, D. M. Stamper-Kurn, C. Gross, and I. Bloch, A subradiant optical mirror formed by a single structured atomic layer, *Nature* **583**, 369 (2020).
- [55] A. Asenjo-Garcia, M. Moreno-Cardoner, A. Albrecht, H. Kimble, and D. E. Chang, Exponential improvement in photon storage fidelities using subradiance and “selective radiance” in atomic arrays, *Phys. Rev. X* **7**, 031024 (2017).

- [56] R. J. Bettles, M. D. Lee, S. A. Gardiner, and J. Ruostekoski, Quantum and nonlinear effects in light transmitted through planar atomic arrays, *Commun. Phys.* **3**, 1 (2020).
- [57] A. Cidrim, T. do Espírito Santo, J. Schachenmayer, R. Kaiser, and R. Bachelard, Photon blockade with ground-state neutral atoms, *Phys. Rev. Lett.* **125**, 073601 (2020).
- [58] C. Parmee and J. Ruostekoski, Bistable optical transmission through arrays of atoms in free space, *Phys. Rev. A* **103**, 033706 (2021).
- [59] A. Cipris, N. Moreira, T. do Espírito Santo, P. Weiss, C. Villas-Boas, R. Kaiser, W. Guerin, and R. Bachelard, Subradiance with saturated atoms: Population enhancement of the long-lived states, *Phys. Rev. Lett.* **126**, 103604 (2021).
- [60] J. Pellegrino, R. Bourgain, S. Jennewein, Y. R. Sortais, A. Browaeys, S. Jenkins, and J. Ruostekoski, Observation of suppression of light scattering induced by dipole-dipole interactions in a cold-atom ensemble, *Phys. Rev. Lett.* **113**, 133602 (2014).
- [61] S. Jennewein, M. Besbes, N. Schilder, S. D. Jenkins, C. Sauvan, J. Ruostekoski, J.-J. Greffet, Y. R. Sortais, and A. Browaeys, Coherent scattering of near-resonant light by a dense microscopic cold atomic cloud, *Phys. Rev. Lett.* **116**, 233601 (2016).
- [62] S. L. Bromley, B. Zhu, M. Bishof, X. Zhang, T. Bothwell, J. Schachenmayer, T. L. Nicholson, R. Kaiser, S. F. Yelin, and M. D. Lukin, *et al.*, Collective atomic scattering and motional effects in a dense coherent medium, *Nat. Commun.* **7**, 1 (2016).
- [63] G. Ferioli, A. Glicenstein, I. Ferrier-Barbut, and A. Browaeys, A non-equilibrium superradiant phase transition in free space, *Nat. Phys.* **19**, 1345 (2023).
- [64] S. J. Masson and A. Asenjo-Garcia, Universality of Dicke superradiance in arrays of quantum emitters, *Nat. Commun.* **13**, 2285 (2022).
- [65] S. P. Pedersen, L. Zhang, and T. Pohl, Quantum nonlinear metasurfaces from dual arrays of ultracold atoms, *Phys. Rev. Res.* **5**, L012047 (2023).
- [66] D. Chang, J. Ye, and M. Lukin, Controlling dipole-dipole frequency shifts in a lattice-based optical atomic clock, *Phys. Rev. A* **69**, 023810 (2004).
- [67] L. Henriet, J. S. Douglas, D. E. Chang, and A. Albrecht, Critical open-system dynamics in a one-dimensional optical-lattice clock, *Phys. Rev. A* **99**, 023802 (2019).
- [68] C. Qu and A. M. Rey, Spin squeezing and many-body dipolar dynamics in optical lattice clocks, *Phys. Rev. A* **100**, 041602 (2019).
- [69] A. D. Ludlow, M. M. Boyd, J. Ye, E. Peik, and P. O. Schmidt, Optical atomic clocks, *Rev. Mod. Phys.* **87**, 637 (2015).
- [70] H. Carmichael, *An Open Systems Approach to Quantum Optics: Lectures Presented at the Université Libre de Bruxelles, October 28 to November 4, 1991* (Springer Science & Business Media, Springer Berlin, Heidelberg, 2009), Vol. 18.